Coherent Bremsstrahlung and Pair Production in the Diamond Crystal in Graphical Representation between 1 and 40 GeV

G. Lutz and U. Timm

Deutsches Elektronen-Synchrotron DESY, Hamburg

(Z. Naturforschg. **21 a**, 1976—1987 [1966]; received 27 May 1966)

The paper supplies numerical information on coherent effects of bremsstrahlung and electron pair production in diamond crystals in the energy range from 1 to 40 GeV. The information is collected in a number of graphs and tables showing the intensity and polarization of bremsstrahlung and the cross section and asymmetry ratio for pair production as a function of crystal orientation. The basic formulas for the interpretation of the diagrams are given. The experimental problem of a precise orientation of the crystal, which is closely connected with the production of coherent radiation, is discussed on the basis of these formulas.

The production of coherent bremsstrahlung (BS) and pair production (PP) from a monocrystal target has been investigated by various authors theoretically [1–5] and experimentally [6–10]. For special orientations of the electron beam with respect to the crystal lattice one obtains photons with a high degree of linear polarization and a spectrum with a number of quasi-monochromatic lines, which is strongly enhanced in intensity as compared to the values obtained with a normal target. Both these features are significant for photoproduction experiments at high energies. In view of an expanding application of this technique in several high energy laboratories it seemed useful to collect numerical data concerning intensity distribution and polarization effects of BS and PP in crystals, and plot it in a universally useful form, covering a wide range of energies and angular orientations. This has been done here for the case of a diamond crystal. The coherent effects – usually called Überall–Diambrini effect after the two most important contributions to this problem – also provide means of finding the correct orientation of the crystal, which is a very important requirement for the application. This technique is described.

1. Geometrical and Kinematical Definitions

We consider an electron or photon beam with momentum $\boldsymbol{p}_0$ or $\boldsymbol{k}_0$, energy E_0 or k_0, striking a diamond crystal at a small angle Θ with respect to its axis $\boldsymbol{b}_1 = [110]$, see Fig. 1. It is assumed in this paper that $\Theta \ll 1$. We further choose α to be the angle between the planes $\boldsymbol{p}_0$, [110] (BS) or $\boldsymbol{k}_0$, [110] (PP) and [001], [110]. This choice of orientation is, of course, arbitrary but fixed for the information presented in this paper. The primary beam shall have no divergence, and the target thickness shall be small to the extent that multiple scattering of the electrons is negligible. Also we assume the diamond to have a perfect lattice. These idealized conditions can be fulfilled to a good approximation in experimental practice.

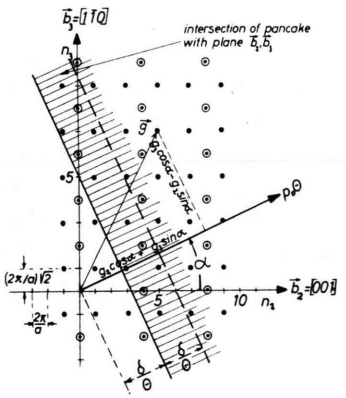

Fig. 1. Projection of $\boldsymbol{p}_0$ into the reciprocal latice plane $\boldsymbol{b}_2$, $\boldsymbol{b}_3$ of the diamond.

[1] B. Ferretti, Nuovo Cim. **7**, 118 [1950].
[2] M. L. Ter Mikaelyan, Zh. Eksperim. Teor. Fiz. **25**, 296 [1953].
[3] H. Überall, Phys. Rev. **103**, 1055 [1956].
[4] G. Barbiellini, G. Bologna, G. Diambrini, and G. P. Murtas, Phys. Rev. Letters **8**, 112 [1962].
[5] H. Überall, Z. Naturforschg. **17 a**, 332 [1962].
[6] O. R. Frisch and D. H. Olsen, Phys. Rev. Letters **3**, 141 [1959].
[7] G. Barbiellini, G. Bologna, G. Diambrini, and G. P. Murtas, Phys. Rev. Letters **8**, 454 [1962].
[8] S. Kato, T. Kifune, Y. Kimura, M. Kobayashi, K. Kondo, T. Nishikawa, H. Sasaki, K. Takamatsu, S. Kikuta, and K. Kohra, J. Phys. Soc. Japan **20**, 203 [1965].
[9] G. Bologna, G. Lutz, H. D. Schulz, U. Timm, and W. Zimmermann, Nuovo Cim. **42**, 844 [1966].
[10] G. Bologna, G. Lutz, H. D. Schulz, U. Timm, and W. Zimmermann, Proc. Intern. Symp. on Electron and Photon Interactions at High Energies, Vol. II, 455 [1965].

The momentum space for the two processes

$$e^- + N \rightarrow N + e^- + \gamma \qquad \text{(BS)}$$

$$\gamma + N \rightarrow N + e^+ + e^- \qquad \text{(PP)}$$

is the reciprocal lattice of the crystal, here given by the crystal axes $\boldsymbol{b}_1 = [110]$, $\boldsymbol{b}_2 = [001]$, $\boldsymbol{b}_3 = [1\bar{1}0]$. The recoil momenta $\boldsymbol{q}$ of the nuclei are restricted to a very thin disc-shaped region perpendicular to $\boldsymbol{p}_0$ or $\boldsymbol{k}_0$, called "pancake" by ÜBERALL, the lower and sharp boundary being a distance δ away from the origin. δ is the minimum momentum transfer to the nucleus, in units of Mc. For BS

$$\delta = \frac{Mc^2}{2E_0} \cdot \frac{x}{1-x} \qquad \text{(BS)} \qquad (1)$$

where M equals the electron mass, and $x = k/E_0$ is the relative quantum energy. In the case of pair production the minimum momentum transfer is given by

$$\delta = \frac{Mc^2}{2k_0} \cdot \frac{1}{y(1-y)} \qquad \text{(PP)} \qquad (2)$$

where $y = E^+/k_0$ is the relative energy of one particle in the pair.

The upper boundary of this kinematical region is not sharp, but the thickness of the disc is roughly δ. Contributions to the cross section of the processes in question come from points inside this region only. For a crystal these are the discrete manifold of inverse lattice vectors which represent the lattice planes of the actual crystal. If Θ is small this region intersects the plane $\boldsymbol{b}_2$, $\boldsymbol{b}_3$ perpendicular to $\boldsymbol{b}_1$ in an area of thickness δ/Θ at the same distance from the origin. This situation is illustrated in Fig. 1, shaded area, where the plane $\boldsymbol{b}_2$, $\boldsymbol{b}_3$ of the reciprocal lattice is shown, as well as the projection of $\boldsymbol{p}_0$ into this plane and the discrete reciprocal lattice points, each being the endpoint of a vector $\boldsymbol{g}$ with components g_2, g_3 in this plane, where

$$g_2 = \frac{2\pi}{a} n_2, \qquad g_3 = \frac{2\pi}{a}\sqrt{2}\, n_3, \qquad (3)$$

and $a = 922$ is the edge of the fundamental cube of the diamond in units of $\lambda_c/2\pi$, λ_c being the COMPTON wave length of the electron. The definition of (n_2, n_3) is given in Fig. 1. These indices are choosen for convenience here. It should be noted that the proper MILLER indices in the plane $n_1 = 0$ are the triplet $(n_3, \bar{n}_3, n_2)$. Inverse lattice planes with $g_1 \neq 0$ are not considered, because they give negligible contributions with the assumption of Θ being small. The reciprocal lattice points have weights $|S|^2 = 32$ for the points and $|S|^2 = 64$ for the circles in Fig. 1.

2. Cross Sections for Bremsstrahlung and Pair Production

2.1 Formulas for coherent bremsstrahlung

The BS intensity integrated over all emission angles is given by [7]

$$I(x, E_0, \Theta, \alpha) \equiv \frac{x}{N\bar{\sigma}} \frac{d\sigma}{dx} = [1 + (1-x)^2][\psi_1(\delta, \Theta, \alpha) + \psi_1^{\,i}(\delta)] - \tfrac{2}{3}(1-x)\,[\psi_2(\delta, \Theta, \alpha) + \psi_2^{\,i}(\delta)], \qquad (4)$$

where N is the number of atoms in the crystal, $\bar{\sigma} = (Z^2/137)(e^2/Mc^2) = 2.09 \cdot 10^{-26}$ cm^2 for carbon. The functions $\psi_{1,2}^i(\delta)$ show very little variation with δ [3] in the region of interest where δ is very small and are assumed to be constant. At $\delta = 0$:

$$\psi_1^{\,i} = 18.2, \qquad \psi_2^{\,i} = 17.4\,. \qquad (5)$$

$\psi_{1,2}^i(0)$ have been calculated from the appropriate integral given in [3] but using scattering factors published by CROMER and WABER [11]. Also the contributions of the electrons, assumed to be incoherent and therefore calculated after WHEELER and LAMB [12], are included in (5). These constants form the incoherent part of the intensity, which is due to thermal lattice vibrations:

$$I^i(x) = [1 + (1-x)^2] \cdot 18.2 - \tfrac{2}{3}(1-x) \cdot 17.4\,. \qquad (6)$$

The incoherent contribution (6) is represented in Fig. 2 as a function of x.

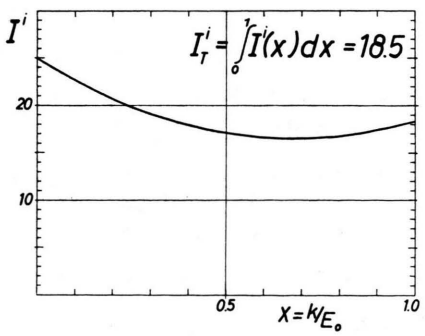

Fig. 2. Bremsstrahlung, incoherent intensity as a function of x.

[11] D. T. CROMER and J. T. WABER, Acta Cryst. **18**, 104 [1965].

[12] J. A. WHEELER and W. E. LAMB, Phys. Rev. **55**, 858 [1939].

The functions ψ_1, ψ_2 in (4) are given by [13] as

$$\psi_1(\delta,\Theta,\alpha) = \frac{N_0}{N}\frac{(2\pi)^2}{a^3}\frac{4\delta}{\Theta^2} \cdot \sum_{(g)} |S|^2 e^{-Ag^2} C(g^2) \frac{g_2^2+g_3^2}{(g_2\cos\alpha+g_3\sin\alpha)^2},$$

$$\psi_2(\delta,\Theta,\alpha) = \frac{N_0}{N}\frac{(2\pi)^2}{a^3}\frac{24\delta^2}{\Theta^3} \cdot \sum_{(g)} |S|^2 e^{-Ag^2} C(g^2) \frac{(g_2^2+g_3^2)(g_2\cos\alpha+g_3\sin\alpha-\delta/\Theta)}{(g_2\cos\alpha+g_3\sin\alpha)^4} \quad (7)$$

where $N/N_0 = 8$ is the number of atoms in the fundamental cell, $A = 126$ is the mean square temperature displacement of the carbon nuclei at room temperature, δ is defined by Eq. (2), a and $|S|^2$ are defined below Eq. (3), and $C(g^2)$ is an atomic screening function which is given by

$$C(g^2) = \frac{1}{g^4}\left[1 - \frac{1}{Z}\left\{\sum_{i=1}^{4} a_i \exp(-\bar{b}_i \cdot g^2) + c\right\}\right]^2 \quad (8)$$

where Z is the atomic number, and the constants a_i, $b_i = (2\lambda_c)^2 \bar{b}_i$ and c are taken for carbon from ref. [11]:

$$\begin{aligned} a_1 &= 1.8359, & \bar{b}_1 &= 1.0528\cdot 10^4, \\ a_2 &= 1.8119, & \bar{b}_2 &= 0.4678\cdot 10^4, \\ a_3 &= 1.5809, & \bar{b}_3 &= 0.0239\cdot 10^4, \\ a_4 &= 0.5426, & \bar{b}_4 &= 2.7116\cdot 10^4, \\ & & c &= 0.2283\,. \end{aligned} \quad (8')$$

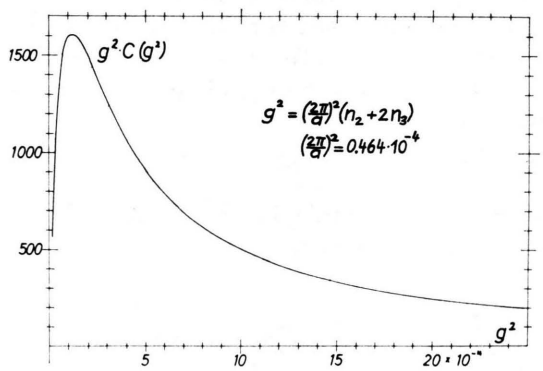

Fig. 3. Atomic screening function $g^2 \cdot C(g^2)$ as a function of g^2, for carbon. g in units $2\pi/\lambda_c$.

$g^2 \cdot C(g^2)$ for carbon is plotted in Fig. 3. The sum (g) in (7) is to be taken of those reciprocal lattice vectors only which satisfy the condition

$$0 \leqq \delta/\Theta \leqq g_2\cos\alpha + g_3\sin\alpha\,. \quad (9)$$

The polarization is linear and is defined as the difference of intensities with the photon electric vectors perpendicular and parallel respectively to a plane Π, divided by the sum:

$$P_\Pi = \frac{I_{\perp\Pi} - I_{\parallel\Pi}}{I_{\perp\Pi} + I_{\parallel\Pi}} = \frac{2(1-x)\,\psi_3(\delta,\Theta,\alpha,\varphi)}{I(x,E_0,\Theta,\alpha)} \quad (10)$$

where

$$\psi_3(\delta,\Theta,\alpha,\varphi) = -\frac{N_0}{N}\frac{(2\pi)^2}{a^3}\frac{4\delta^3}{\Theta^4} \cdot \sum_{(g)} |S|^2 e^{-Ag^2} C(g^2) \frac{(g_2^2-g_3^2)\cos 2\varphi + 2g_2 g_3 \sin 2\varphi}{(g_2\cos\alpha+g_3\sin\alpha)^4}. \quad (11)$$

The reference plane Π contains $\boldsymbol{p}_0$ and lies at angle φ with respect to plane $\boldsymbol{p}_0$, [001]. For $\varphi = \alpha$ this plane is given by $\boldsymbol{p}_0$, [110], which is used as a fixed reference plane in [13]. It should be noted that this definition is valid in the limit $\Theta \ll 1$, where $\boldsymbol{p}_0$ and [110] have nearly the same direction.

2.2. Formulas for coherent pair production

The cross section for coherent PP in a diamond crystal, as taken from [13], is given by

$$J(y,k_0,\Theta,\alpha) = \frac{1}{N\sigma}\frac{d\sigma}{dy} = [y^2+(1-y)^2]\,[\psi_1(\delta,\Theta,\alpha)+\psi_1^{\,i}(\delta)] + \tfrac{2}{3}y(1-y)\,[\psi_2(\delta,\Theta,\alpha)+\psi_2^{\,i}(\delta)], \quad (12)$$

where y is defined in connection with Eq. (2) and $\psi_{1,2}^i$, $\psi_{1,2}$ are given by (5) and (7), keeping in mind that δ is now defined by (2).

In the place of the polarization P for BS we define for PP the asymmetry ratio R, following [13], as:

$$R = \frac{J_{\perp\Pi} - J_{\parallel\Pi}}{J_{\perp\Pi} + J_{\parallel\Pi}} = \frac{2y(1-y)\,\psi_3(\delta,\Theta,\alpha,\varphi)}{J(y,k_0,\Theta,\alpha)}. \quad (13)$$

$J_{\perp\Pi}$ and $J_{\parallel\Pi}$ represent the differential PP cross sections resulting from photons completely polarized perpendicular and parallel, respectively, to the plane Π defined in the foregoing paragraph, but with $\boldsymbol{p}_0$ replaced by $\boldsymbol{k}_0$.

2.3. Universal representation

If we express δ in Eq. (7) by Eq. (1), then the function ψ_1 can be written in the following form:

$$\psi_1 = \frac{E_0}{(\Theta E_0)^2}\frac{\pi^2 M c^2}{a^3}\frac{x}{1-x} \cdot \sum_{(g)} |S|^2 e^{-Ag^2} C(g^2) \frac{g_2^2+g_3^2}{(g_2\cos\alpha+g_3\sin\alpha)^2}. \quad (14)$$

Similarly, we can write Eq. (9), the limit of summation, as:

$$\frac{1}{\Theta E_0}\frac{x}{1-x}\frac{Mc^2}{2} \leqq g_2\cos\alpha + g_3\sin\alpha\,. \quad (15)$$

[13] G. Bologna, G. Barbiellini, G. Diambrini, and G. P. Murtas, Nuovo Cim. **28**, 435 [1963].

This shows that ψ_1 is proportional to E_0, and that it can be written as a function of α, x and ΘE_0. The same applies to ψ_2 and ψ_3.

Therefore the intensity, Eq. (4), can be split into an incoherent part $I^i(x)$, Eq. (6), which depends on x only, and a coherent part $I^c(x, \Theta E_0, \alpha)$, which is proportional to E_0 and depends on x, ΘE_0, and α, so as to yield a universal representation for I:

$$I(x, E_0, \Theta E_0, \alpha) = I^i(x) + E_0 \cdot I^c(x, \Theta E_0, \alpha). \quad \text{(BS)} \quad (16)$$

The same is true for the polarization P as given by Eq. (10):

$$P(x, E_0, \Theta E_0, \alpha, \varphi) = \frac{2(1-x) \cdot E_0 \cdot p(x, \Theta E_0, \alpha, \varphi)}{I^i(x) + E_0 \cdot I^c(x, \Theta E_0, \alpha)}; \quad p \equiv \psi_3 / E_0. \quad (17)$$

Further, expressing δ in Eq. (7) by Eq. (2) an analogous dependence results for PP, Eqs. (12) and (13) take the general form:

$$J(y, k_0, \Theta k_0, \alpha) = J^i(y) + k_0 \cdot J^c(y, \Theta k_0, \alpha); \quad \text{(PP)} \quad (18)$$

$$R(y, k_0, \Theta k_0, \alpha, \varphi) = \frac{2y(1-y) \cdot k_0 \cdot r(y, \Theta k_0, \alpha, \varphi)}{J^i(y) + k_0 \cdot J^c(y, \Theta k_0, \alpha)}; \quad r \equiv \psi_3 / k_0. \quad (19)$$

Because of this general behaviour, the functions I, P, J, R can be presented as diagrams, which are useful for the experimental application of the ÜBERALL–DIAMBRINI effect.

3. Intensity of Bremsstrahlung as a Function of x

First we deal with the two significant cases $\alpha = 0°$ and 90°, where the pancake intersection is parallel to $\boldsymbol{b}_3$ and $\boldsymbol{b}_2$ respectively.

3.1. Case $\alpha = 0°$

In this case inequality (15) reduces to

$$\frac{1}{\Theta E_0} \frac{M c^2}{2} \frac{x}{1-x} \leqslant \frac{2\pi}{a} n_2. \quad (20)$$

The coherent spectrum is rather well determined by its intensity steps at the discontinuities, for which the equality sign in Eq. (20) is valid. From Eq. (20) the positions x_d of the discontinuities are determined by

$$x_d = \frac{1}{1 + a M c^2 / (4\pi n_2 \Theta E_0)}, \quad (21)$$

$$\Theta E_0 = \frac{a M c^2}{4\pi n_2} \frac{x_d}{1-x_d}, \quad n_2 = 1, 3, 4, 5, 7, 8, 9, \ldots .$$

If Θ is measured in mrad, E_0 in GeV, we find

$$\frac{a M c^2}{4\pi} = 37.49 \cdot 10^{-3} \text{ GeV}. \quad (22)$$

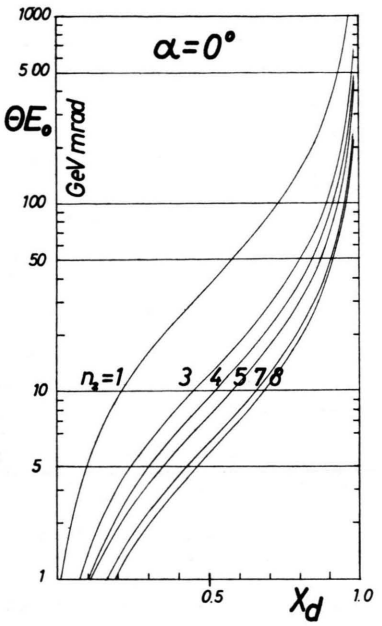

Fig. 4. Bremsstrahlung, discontinuities as a function of ΘE_0, $\alpha = 0°$. Correction: 5 on the vertical axis to be replaced by 4.

x_d as a function of E_0 is plotted in Fig. 4. At the discontinuities the intensity (16) depends only on x_d, because of relation (21). It is a double valued function of x_d, which we denote by u = upper value and l = lower value:

$$\begin{aligned} I^u &= I^i(x_d) + E_0 I^{cu}(x_d, 0), \\ I^l &= I^i(x_d) + E_0 I^{cl}(x_d, 0), \\ \Delta I &= I^u - I^l = E_0 \Delta I^c(x_d, 0). \end{aligned} \quad (23)$$

The universal functions $I^{cl}(x_d, 0)$ and, for convenience of representation, the intensity step

$$\Delta I^c(x_d, 0) = I^{cu} - I^{cl}$$

are plotted in Fig. 5 in units GeV^{-1}. It is possible to construct from these curves a coherent spectrum for any given situation, as the following example will illustrate.

Example: Let the electron energy available be $E_0 = 2$ GeV. We want the first peak of the spectrum to lie at 600 MeV, so that $n_2 = 1$, $x_d = 0.3$. Fig. 4 gives $\Theta E_0 = 16$ and therefore $\Theta = 8$ mrad. From the same plot we derive the discontinuity positions for $n_2 = 3$, 4, 5, 7. The auxiliary data necessary to evaluate the spectrum are given in Table 1. The first line contains the discontinuity numbers n_2. The next line lists the values x_d from

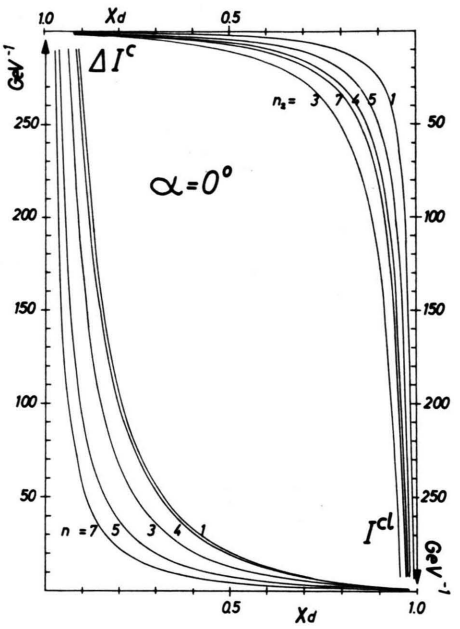

Fig. 5. Bremsstrahlung, intensity steps and lower intensity as a function of x_d, $\alpha=0°$.

Fig. 4. The following two lines contain ΔI^c and I^{cl} from Fig. 5, from which I^{cu} is calculated in line number five. I^{cu} and I^{cl} have to be multiplied by E_0 and $I^i(x_d)$ from Fig. 2 added to give I^u, I^l which are listed in the last two lines.

The spectrum can now be constructed as indicated in Fig. 6 and completed by drawing the dotted lines.

3.2. *Case* $\alpha = 90°$

For the position of discontinuities we now find from Eq. (15)

$$x_d = \frac{1}{1+a\,M\,c^2/(4\,\pi\,n_3\sqrt{2}\,\Theta\,E_0)}\,, \tag{24}$$

$$\Theta\,E_0 = \frac{a\,M\,c^2}{4\,\pi\,n_3\sqrt{2}}\,\frac{x_d}{1-x_d}\,, \qquad n_3 = 1, 2, 3, 4, \ldots\,,$$

$$a\,M\,c^2/(4\,\pi\,\sqrt{2}) = 26.51\cdot 10^{-3}\ \text{GeV}. \tag{25}$$

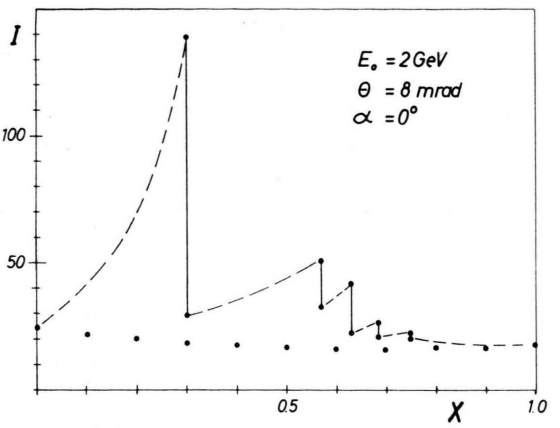

Fig. 6. Coherent BS spectrum constructed from Figs. 2, 4, 5 for $E_0=2$ GeV, $\Theta=8$ mrad, $\alpha=0°$.

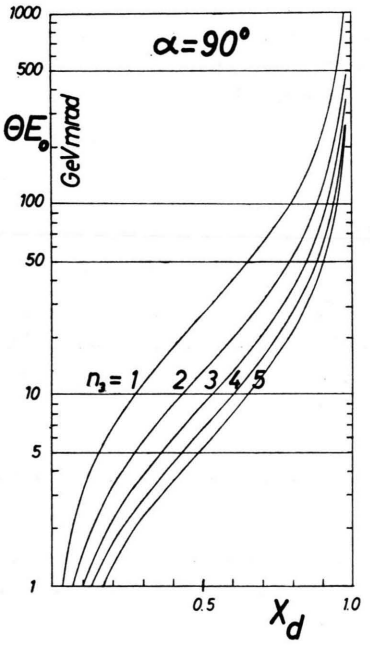

Fig. 7. Bremsstrahlung, discontinuities as a function of $\Theta\,E_0$, $\alpha=90°$.

(1)	n_2	1	3	4	5	7	
(2)	x_d	0.300	0.570	0.630	0.683	0.750	Fig. 4
(3)	ΔI^c	55.2	9.0	10.0	3.0	1.3	Fig. 5
(4)	I^{cl}	5.4	8.0	2.6	2.2	2.0	Fig. 5
(5)	I^{cu}	60.6	17.0	12.6	5.2	3.3	(3) + (4)
(6)	$E_0\,I^{cu}$	121.2	34.0	25.2	10.4	6.6	(5) · E_0
(7)	$E_0\,I^{cl}$	10.8	16.0	5.2	4.4	4.0	(4) · E_0
(8)	I^i	19.0	16.7	16.5	16.4	16.5	Fig. 2
(9)	I^u	140.2	50.7	41.7	26.8	23.1	(6) + (8)
(10)	I^l	29.8	32.7	21.7	20.8	20.5	(7) + (8)

Table 1. BS, $\alpha=0°$, $\Theta=8$ mrad, $E_0=2$ GeV.

x_d is plotted in Fig. 7 against ΘE_0 for $\alpha = 90°$. The intensity functions I^{cl} and ΔI^c are plotted in Fig. 8 in units of GeV^{-1}. With the aid of Figs. 7 and 8 the spectrum for $\alpha = 90°$ is constructed in the same manner as has been described for $\alpha = 0°$.

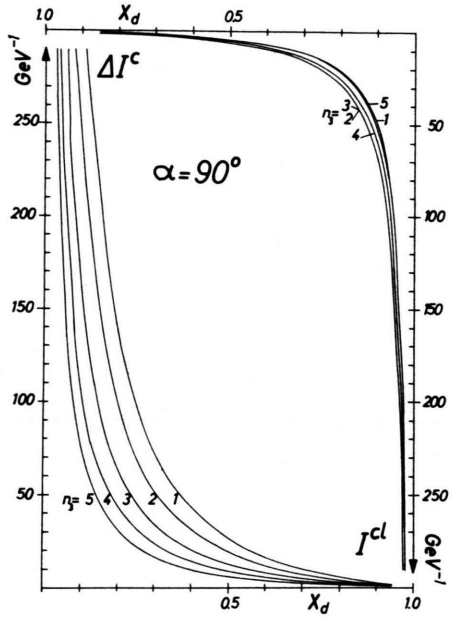

Fig. 8. Bremsstrahlung, intensity steps and lower intensity as a function of x_d, $\alpha = 90°$.

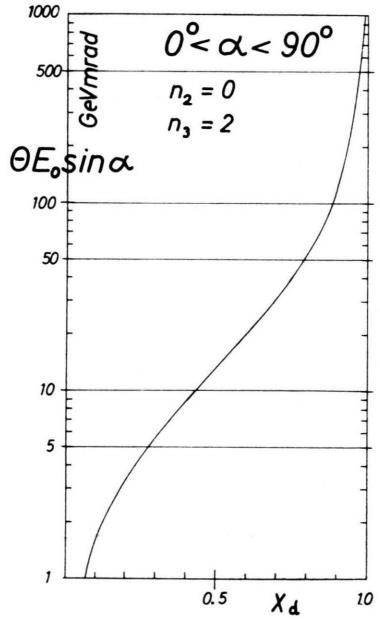

Fig. 9. Bremsstrahlung, position of discontinuity for the lattice point (0,2) as a function of $\Theta E_0 \sin\alpha$, $0° < \alpha < 90°$.

3.3. Case $0° < \alpha < 90°$

In this case the relation (15), with equality sign, gives the positions of all possible discontinuities in the spectrum. We write this equation now in the form

$$x_d = 1 \Big/ \left(1 + \frac{a\, M\, c^2}{4\,\pi\,\Theta\, E_0 (n_2 \cos\alpha + n_3 \sqrt{2} \sin\alpha)}\right), \qquad (26)$$

with Θ in mrad, E_0 in GeV. Fig. 9 gives x_d as a function of $\Theta E_0 \sin\alpha$ for the most important inverse lattice point 0.2).

The intensity steps ΔI^c are now determined by single inverse lattice points because – as α is neither $0°$ nor $90°$ – with increasing x in general only single points are lost from the pancake instead of rows of points. From Eq. (7) and (4) we find the relation for an intensity step at the discontinuity x_d, which does not depend on α:

$$\Delta I^c = \frac{1-x_d}{x_d}\left[1 + (1-x_d)^2\right] \frac{8\,N_0}{N} \frac{(2\,\pi)^4}{a^5\, M\, c^2} \qquad (27)$$
$$|S|^2\, e^{-Ag^2}\, C(g^2)\, (n_2^2 + 2\, n_3^2).$$

As $g^2\, C(g^2)\, e^{-Ag^2}$ is a function which is strongly peaked around the origin of the reciprocal lattice space, the intensity steps are large for points in the vicinity of the origin, like (0,2), (1,1), (4,0), (4,2), (3,1), (1,3). ΔI^c is plotted for the most important inverse lattice point (0,2) in Fig. 10. In addition Fig. 10 shows the lower intensity I^{cl} for some values of α.

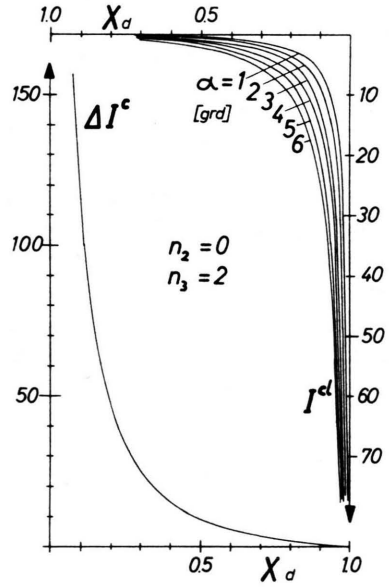

Fig. 10. Bremsstrahlung, intensity step and lower intensity for the lattice point (0,2), as a function of x_d, $1° \leqq \alpha \leqq 6°$.

The importance of the single point steps from the experimental point of view lies in the fact that they have high polarisation, as will become evident in paragraph 6. In order to obtain spectra where the contribution from a single point dominates the spectrum one must meet two conditions: (1) The pancake intersection thickness, δ/Θ, must be small, which can be done, as Fig. 1 shows, by increasing Θ. (2) α must be chosen such that the point wanted is included in the intersection area of the pancake. If these conditions are met, the spectrum can be constructed by using I^{cl} and ΔI^{c} from Fig. 10 in connection with $I^{\mathrm{i}}(x)$ from Fig. 2, the peak position being determined by Eq. (26). The most suitable point with respect to intensity and polarization is (0,2), which is obtained for large Θ and small $\alpha \neq 0$.

4. Integrated Intensity of Bremsstrahlung

In order to obtain the total intensity from a coherent spectrum we have to integrate Eq. (4) over x. The knowledge of the dependence of the total intensity from the parameters Θ, E_0 and α is necessary for experiments where the coherent γ-radiation is monitored by a quantameter.

Following Eq. (16) the total intensity may be split into two parts:

$$I_{\mathrm{T}}(E_0, \Theta E_0, \alpha) = I_{\mathrm{T}}^{\mathrm{i}} + E_0 I_{\mathrm{T}}^{\mathrm{c}}(\Theta E_0, \alpha). \quad (28)$$

The incoherent contribution can be derived from Eq. (6):

$$I_{\mathrm{T}}^{\mathrm{i}} = \int_0^1 I^{\mathrm{i}}(x)\, \mathrm{d}x = \tfrac{4}{3}\psi_1^{\mathrm{i}} - \tfrac{1}{3}\psi_2^{\mathrm{i}} = 18.5\,. \quad (29)$$

In order to understand the procedure of integration for the coherent part we first imagine that the reciprocal lattice plane $\boldsymbol{b}_2$, $\boldsymbol{b}_3$ contains only one $\boldsymbol{g}$ so that the sum in Eq. (7) can be omitted. Expressing δ then by Eq. (1) we find for the total intensity arising from the point $\boldsymbol{g}$:

$$I_{\mathrm{T}}^{\mathrm{c}} = \int_0^1 I^{\mathrm{c}}(x, \Theta E_0, \alpha)\, \mathrm{d}x = \frac{N_0}{N}\frac{(2\pi)^2}{a^3}\frac{2Mc^2}{(\Theta E_0)^2}\cdot\Bigg[\int_0^1 \frac{x[1+(1-x)^2]}{1-x}\,|S|^2 e^{-Ag^2} C(g^2)\,\frac{(g_2^2+g_3^2)\,\mathrm{d}x}{(g_2\cos\alpha + g_3\sin\alpha)^2}$$

$$-\frac{2Mc^2}{\Theta E_0}\int_0^1 \frac{x^2}{1-x}\,|S|^2 e^{-Ag^2} C(g^2)\,\frac{(g_2^2+g_3^2)\,\mathrm{d}x}{(g_2\cos\alpha + g_3\sin\alpha)^3} \quad (30)$$

$$+\left(\frac{Mc^2}{\Theta E_0}\right)^2\int_0^1 \frac{x^3}{(1-x)^2}\,|S|^2 e^{-Ag^2} C(g^2)\,\frac{(g_2^2+g_3^2)\,\mathrm{d}x}{(g_2\cos\alpha + g_3\sin\alpha)^4}\Bigg].$$

Under each of the three integrals the condition (9) holds. This means – following Eq. (15) and (26) – that $\boldsymbol{g}$ only contributes to the intensity, if

$$x \leqq x_{\mathrm{d}} = 1\Big/\left(1 + \frac{Mc^2}{2\Theta E_0(g_2\cos\alpha + g_3\sin\alpha)}\right). \quad (31)$$

Therefore the upper limit of the integral has to be replaced by x_{d}. In the actual reciprocal lattice plane we now have to sum up all these individual contributions, so that the result is an interchange of summation and integration:

$$I_{\mathrm{T}}^{\mathrm{c}} = \frac{N_0}{N}\frac{(2\pi)^2}{a^3}\frac{2Mc^2}{(\Theta E_0)^2}\sum_{(g)}|S|^2 e^{-Ag^2} C(g^2)(g_2^2+g_3^2)\sum_{i=1}^{3}\frac{A_i(x_{\mathrm{d}})}{(g_2\cos\alpha + g_3\sin\alpha)^{i+1}},$$

$$A_1(x_{\mathrm{d}}) = \int_0^{x_{\mathrm{d}}} \frac{x[1+(1-x)^2]}{1-x}\,\mathrm{d}x = -\ln(1-x_{\mathrm{d}}) - x_{\mathrm{d}} + \frac{x_{\mathrm{d}}^2}{2} - \frac{x_{\mathrm{d}}^3}{3},$$

$$A_2(x_{\mathrm{d}}) = -\frac{2Mc^2}{\Theta E_0}\int_0^{x_{\mathrm{d}}} \frac{x^2\,\mathrm{d}x}{1-x} = \frac{2Mc^2}{\Theta E_0}\left(\ln(1-x_{\mathrm{d}}) + x_{\mathrm{d}} + \frac{x_{\mathrm{d}}^2}{2}\right), \quad (32)$$

$$A_3(x_{\mathrm{d}}) = \left(\frac{Mc^2}{\Theta E_0}\right)^1\int_0^{x_{\mathrm{d}}} \frac{x^3\,\mathrm{d}x}{(1-x)^2} = \left(\frac{Mc^2}{\Theta E_0}\right)^2\left(3\ln(1-x_{\mathrm{d}}) + 2x_{\mathrm{d}} + \frac{x_{\mathrm{d}}^2}{2} + \frac{x_{\mathrm{d}}}{1-x_{\mathrm{d}}}\right).$$

The sum in (32) is now taken over all lattice points in the half plane $x_d \geqq 0$ or, in terms of components g_2, g_3:

$$(g_2 \cos\alpha + g_3 \sin\alpha) = \frac{M c^2}{2\,\Theta E_0}\,\frac{x_d}{1-x_d} \geqq 0\,. \quad (33)$$

If α is chosen such that reciprocal lattice points lie on the lower boundary $x_d = 0$ of the pancake, then these points appear symmetric with respect to the origin. For an exact result the summation in (32), however, includes only half of these points. This can be seen from the asymptotic behaviour if we change α by $\pm\Delta\alpha$. An equivalent argument arises from the fact that the lower pancake boundary is not really a plane but is slightly curved; therefore the symmetry argument actually is not valid. Also, at a first glance, the sum of Eq. (32) appears to approach infinity for $x \to 0$. However, by expanding $\ln(1-x_d)$ and $x_d/(1-x_d)$ one can show that

$$\lim_{x_d \to 0} \sum_{i=1}^{3} \frac{A_i(x_d)}{(g_2 \cos\alpha + g_3 \sin\alpha)^{i+1}} = \frac{8}{3}\left(\frac{\Theta E_0}{M c^2}\right)^2. \quad (34)$$

The coherent part of the total intensity is plotted in Fig. 11 as a function of ΘE_0 and α in polar coordinates with the parameter $I_T{}^c$, in GeV^{-1}. Fig. 12 shows $I_T{}^c$ versus ΘE_0 for $\alpha = 0°$, $90°$. The integrated intensity as a function of E_0, Θ and α is derived from these plots in connection with Eq. (28) and (29).

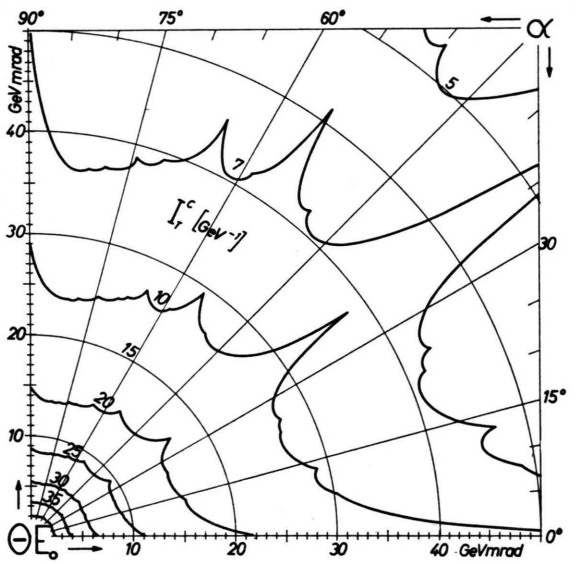

Fig. 11. Coherent part of total intensity as a function of ΘE_0 and α.

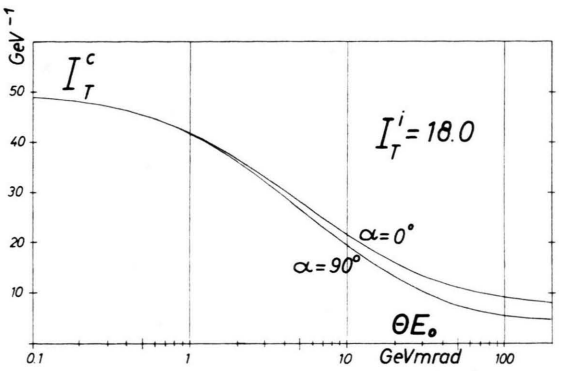

Fig. 12. Coherent part of total intensity as a function of ΘE_0 for $\alpha = 0°$, $90°$. Correction: $I_T{}^i = 18.5$.

5. Intensity of Bremsstrahlung as a Function of Θ

For the alignment of the crystal with respect to the electron beam it is necessary to measure the intensity as a function of Θ, with E_0 and x fixed. This distribution may be constructed like the spectra with the aid of Figs. 2, 4, 5, 7, 8 for $\alpha = 0°$ or $90°$, whichever case applies. The position of the discontinuities, which we call Θ_d now, are taken from Fig. 4 or 7, and the coherent intensity steps from Fig. 5 or 8, which are then combined after Eq. (16) to give the intensity distribution $I(x, E_0, \Theta E_0, \alpha)$, which is symmetric in Θ. This, however, is not the quantity actually measured because, using a pair spectrometer, the coherent γ-ray serves at the same time as a monitor of the counts. The observed quantity is therefore rather:

$$\frac{I(x, E_0, \Theta E_0, \alpha)}{I_T(E_0, \Theta E_0, \alpha)} = \frac{I^i(x) + E_0\, I^c(\Theta_d E_0, \alpha)}{I_T{}^i + E_0\, I_T{}^c(\Theta_d E_0, \alpha)}\,, \quad (35)$$

where the total intensity is taken from Fig. 11 or 12.

6. Polarization of Bremsstrahlung in the First Peak

The polarization is the most significant property of the coherent BS. Its energy dependence resembles that of the intensity, but it is large only at the first peak of the spectrum, i. e., at the lowest discontinuity in energy. Only this maximum polarization is represented here.

Let x_1 be the position of the first discontinuity, P^* the polarization at this peak. The polarization is then

given in accordance with Eq. (17) by the general form:

$$P^*(x_1, E_0, \alpha, \varphi) = \frac{2E_0(1-x_1)\, p^*(x_1, \alpha, \varphi)}{I^{\mathrm{i}}(x_1) + E_0 I^{\mathrm{cu}}(x_1, \alpha)} \qquad (36)$$
$$= \frac{2(1-x_1)\, p^*(x_1, \alpha, \varphi)}{I^{\mathrm{cu}}(x_1, \alpha)} \cdot \frac{1}{1 + I^{\mathrm{i}}(x_1)/E_0 I^{\mathrm{cu}}(x_1, \alpha)} .$$

P^* is plotted in Fig. 13 for the cases $\alpha = \varphi = 0°$, $\alpha = \varphi = 90°$, and $\alpha = 3°$, $\varphi = 0°$, with E_0 as parameter. The general trend is that the polarization increases towards the lower end of the spectrum. The peak position x_1 as a function of ΘE_0 has to be taken from Figs. 4, 7 or 8. The polarization obtained from the orientation $\alpha = 3°$, where, as has been explained in paragraph 3.3, the reciprocal lattice point (0,2) is responsible for the first peak in the spectrum, is much higher than that obtained by any other alignment.

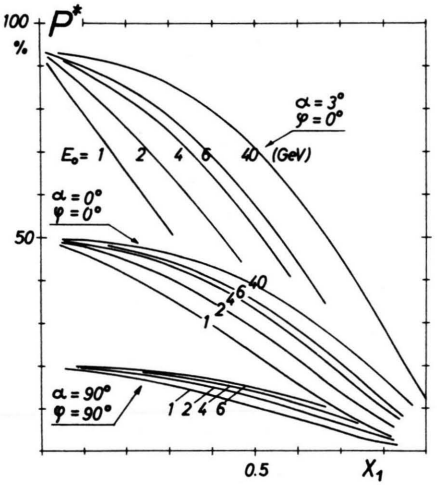

Fig. 13. Polarization of the first peak as function of x_1. $1 \leqq E_0 \leqq 40$ GeV, $\alpha = 0°, 3°, 90°$.

7. Pair Production for $y = 1/2$

Electron pair production by photons is studied in a pair spectrometer. We restrict ourselves here to the case where the observed particles have equal energies, $y = 1/2$. This means that we are only interested in how the cross section for PP is dependent on the angular orientation of the crystal.

According to Eqs. (9), (2) the position of discontinuities Θ_{d} are then given by

$$\Theta_{\mathrm{d}} k_0 = \frac{2Mc^2}{g_2 \cos\alpha + g_3 \sin\alpha} . \qquad (37)$$

The cross section at the discontinuities, resulting from Eq. (18), is represented by the steps:

$$\begin{aligned} J^{\mathrm{u}} &= J^{\mathrm{i}}(\tfrac{1}{2}) + k_0 \cdot J^{\mathrm{cu}}(\tfrac{1}{2}, \alpha), \\ J^{\mathrm{l}} &= J^{\mathrm{i}}(\tfrac{1}{2}) + k_0 \cdot J^{\mathrm{cl}}(\tfrac{1}{2}, \alpha), \\ \Delta J &= J^{\mathrm{u}} - J^{\mathrm{l}} = k_0 \cdot \Delta J^{\mathrm{c}}(\tfrac{1}{2}, \alpha). \end{aligned} \qquad (38)$$

For the incoherent part of (38) one finds from Eqs. (12) and (5):

$$J^{\mathrm{i}}(\tfrac{1}{2}) = \tfrac{1}{2}\psi_1^{\mathrm{i}} + \tfrac{1}{6}\psi_2^{\mathrm{i}} = 12.0 . \qquad (39)$$

The asymmetry ratio (19) is now, for $y = 1/2$:

$$\begin{aligned} R^{\mathrm{u}}(\tfrac{1}{2}) &= k_0 r^{\mathrm{u}}(\tfrac{1}{2}, \alpha, \varphi)/(2J^{\mathrm{u}}); \\ R^{\mathrm{l}}(\tfrac{1}{2}) &= k_0 r^{\mathrm{l}}/(2J^{\mathrm{l}}). \end{aligned} \qquad (40)$$

Eqs. (38) and (40) can be presented in tabular form, which is done for $\alpha = 0°$ (Table 2) and $\alpha = 90°$ (Table 3). As in the case of BS intensity, it is possible with these tables to construct the Θ dependence of the cross section and the asymmetry ratio for PP from the discontinuity values for any value of k_0.

n_2	$\Theta_{\mathrm{d}} k_0$ GeVmrad	J^{cu} GeV^{-1}	J^{cl} GeV^{-1}	$\frac{1}{2} r^{\mathrm{u}}$ GeV^{-1}	$\frac{1}{2} r^{\mathrm{l}}$ GeV^{-1}
1	150.0	2.648	0.437	1.1635	−0.0041
3	50.0	3.467	2.191	−0.3282	−0.1729
4	37.5	3.128	1.241	−0.5465	−0.1316
5	30.0	1.691	0.983	−0.3213	−0.1167
7	21.4	1.598	1.171	−0.4484	−0.2742
8	18.7	1.339	0.661	−0.4676	−0.1604

Table 2. PP, $\alpha = \varphi = 0°$, $y = 1/2$.

n_3	$\Theta_{\mathrm{d}} k_0$ GeVmrad	J^{cu} GeV^{-1}	J^{cl} GeV^{-1}	$\frac{1}{2} r^{\mathrm{u}}$ GeV^{-1}	$\frac{1}{2} r^{\mathrm{l}}$ GeV^{-1}
1	106.0	3.935	1.058	0.5444	−0.0303
2	53.0	3.325	1.398	−0.4840	−0.0860
3	35.3	2.551	1.310	−0.4352	−0.1425
4	26.5	1.944	1.098	−0.4503	−0.1722
5	21.2	1.461	0.864	−0.4204	−0.1778
6	17.7	1.073	0.646	−0.3686	−0.1645

Table 3. PP, $\alpha = \varphi = 90°$, $y = 1/2$.

The coherent PP is in its discontinuous behaviour very similar to the coherent BS. There is one striking difference however, in that the incoherent contribution for PP is very much higher in comparison to the coherent part for comparable energies. The asymmetry ratio is largest for $y = 1/2$. It can be used to analyse polarized photons of high energies [13]. Only the peak $n_2 = 1$ for $\alpha = 0$ is of significance in this respect. For $\alpha \neq 0$ and large Θ but with reciprocal lattice point (0,2) included in the pancake –

in complete analogy to the case treated in paragraph 3.3 for BS – one obtains about the same asymmetry ratio, and even a somewhat higher one for energies above 10 GeV. There is an advantage over the case $\alpha = 0^\circ$ with regard to the magnitude of R^u, which is due to the fact that for $\alpha = 0^\circ$, R^u is sensitive to errors in both angles Θ an α resulting in a reduction from the theoretical value because the peak, originating from a row of lattice points, disintegrates. If, however, R^u originates from the single lattice point (0,2), such a disintegration is not possible.

8. Methods of Crystal Alignment

For the application of the methods described below it is necessary that the position of the axis $\boldsymbol{b}_1$ is known – for instance from X-ray crystallography – within, say, 20 mrad, so that the crystal can be mounted in the goniometer with $\boldsymbol{b}_1$ roughly parallel to $\boldsymbol{p}_0(\boldsymbol{k}_0)$. The precise orientation must be measured in the goniometer itself because an accuracy in the order of 0.1 mrad is required.

We consider the diamond mounted in a goniometer framework which has two axes of rotation $\boldsymbol{f}_2$, $\boldsymbol{f}_3$, perpendicular to each other, by which the crystal can be turned through angles Φ_2, Φ_3 in a small range of perhaps ± 100 mrad. The definition of angles must be good to, say ± 0.1 mrad. The electron or photon beam should be roughly perpendicular to the plane $\boldsymbol{f}_2$, $\boldsymbol{f}_3$. The orientation of the crystal – as measured in the coordinate system Φ_2, Φ_3 – requires the knowledge of the point (Φ_2^0, Φ_3^0) where $\boldsymbol{b}_1$ and $\boldsymbol{p}_0(\boldsymbol{k}_0)$ are parallel and the equation for one of the transverse axes, for instance $\boldsymbol{b}_2$ – i. e. $\boldsymbol{p}_0(\boldsymbol{k}_0)$ in the plane $\boldsymbol{b}_1$, $\boldsymbol{b}_2$ – which may be given by

$$(\Phi_3 - \Phi_3^0) = m(\Phi_2 - \Phi_2^0).$$

If Φ_2^0, Φ_3^0 and m have been determined, we can identify Θ an α in terms of the coordinates Φ_2, Φ_3 by the relations:

$$\Theta = [(\Phi_2 - \Phi_2^0)^2 + (\Phi_3 - \Phi_3^0)^2]^{1/2};\ \Theta \ll 1;$$

$$\operatorname{tg}\alpha = \frac{n-m}{1+n\cdot m};\ n = (\Phi_3 - \Phi_3^0)/(\Phi_2 - \Phi_2^0). \quad (41)$$

The following discussion describes how Φ_2^0, Φ_3^0 and m may be measured by using the angular dependence of either BS or PP.

8.1 Orientation by means of bremsstrahlung

The position (Φ_2^0, Φ_3^0) of the axis $\boldsymbol{b}_1$ can be found by observing the total intensity, for instance with a quantameter, as a function of Φ_2 and Φ_3. It follows from Figs. 11 and 12 in connection with Eq. (28) that the total intensity has a strong peak, proportional to E_0, as Θ approaches zero.

The transverse axes $\boldsymbol{b}_2$, $\boldsymbol{b}_3$ are perpendicular to each other. Therefore it is sufficient to determine one point on one of these axes in addition to (Φ_2^0, Φ_3^0). In practice, of course, one would measure several points. If we assume that $\boldsymbol{b}_2$, $\boldsymbol{b}_3$ are roughly known with respect to their position then we can consider them as mounted nearly parallel to $\boldsymbol{f}_3$, $\boldsymbol{f}_2$, respectively. The BS intensity is now measured at large $\Theta = \text{const}$ as a function of α, which is varied across one of these axes keeping E_0 and x fixed. The intensity thus observed is characterised by two sharp discontinuities which are due to the pairs of inverse lattice points (0,2), $(0,\bar{2})$ or (4,0), $(\bar{4},0)$; each pair lies symmetric to $\boldsymbol{b}_2$ or $\boldsymbol{b}_3$, respectively.

Even if nothing were known about the position of the transverse axes one could find the orientation by observing the pattern of discontinuities which is given in Fig. 14. To understand this pattern, we rewrite Eq. (26) in the following way:

$$A(n_2\,\Theta\cos\alpha + n_3\sqrt{2}\,\Theta\sin\alpha) = 1,$$

$$A = \frac{1-x_d}{x_d}\,\frac{4\,\pi\,E_0}{a\,M\,c^2}, \quad \text{(BS)} \qquad (42)$$

where Θ is measured in mrad, A in mrad^{-1}. For convenience of notation we now assume that $\Phi_{2,3}^0 = 0$ and $m = 0$, which means that the crystal is ideally mounted in the goniometer. It is obvious that Φ_2, Φ_3 are the projections of Θ onto the axes $\boldsymbol{b}_2$, $\boldsymbol{b}_3$:

$$\Phi_2 = \Theta\cos\alpha, \qquad \Phi_3 = \Theta\sin\alpha. \qquad (43)$$

The equation of discontinuities can thus be expressed in the coordinate system of the goniometer in the simple form

$$\frac{A\,\Phi_2}{1/n_2} + \frac{A\,\Phi_3}{1/(n_3\sqrt{2})} = 1. \qquad (44)$$

Eq. (44) shows that each discontinuity from the reciprocal lattice point (n_2, n_3) is represented by a line in the diagram $A\,\Phi_2$, $A\,\Phi_3$, these lines are drawn in Fig. 14 for $|n_2| \leqq 7$ and $|n_3| \leqq 5$. A cross point marks a discontinuity which is caused by a row of points, as in the cases $\alpha = 0^\circ$, 90°. The discontinuity steps descend towards the

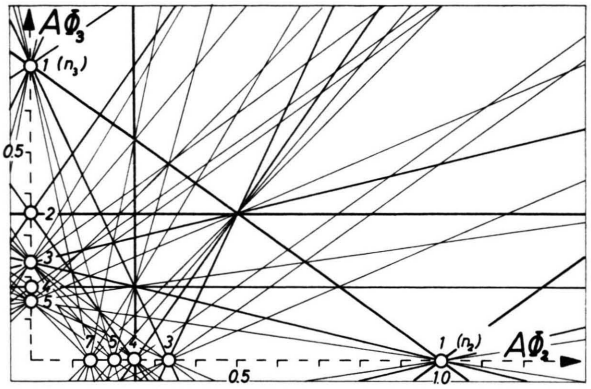

Fig. 14. Lines of discontinuities (n_2, n_3) in the angular space $A\,\Phi_2 = A\,\Theta\cos\alpha$, $A\,\Phi_3 = A\,\Theta\sin\alpha$, $A = E_0(1-x_d)/(37\cdot 49\,x_d)$ for BS, $A = k_0/150.0$ for PP (in mrad^{-1}). E_0, k_0 in GeV, Θ in mrad.

origin of the diagram. Each line is determined by its values on the axes $\boldsymbol{b}_2$, $\boldsymbol{b}_3$ namely $1/n_2$, $1/n_3\sqrt{2}$.

The orientation is now found by observing the coherent photon intensity going along at least two lines for instance $\Phi_2 = \text{const}$, $\Phi_3 = \text{const}$, in the diagram Φ_2, Φ_3. Crossing the discontinuity lines (44) causes characteristic intensity jumps which have to be compared with the pattern of Fig. 14, after the coordinates have been normalized by the factor A.

The step height measured and given by Eq. (27) can also be used to identifiy the discontinuity, although with BS it is usually smaller than the theoretical value due to averaging effects, particularly for small Θ. In this case one has also to take into account the dependence on total intensity, cf. paragraph 5.

8.2 Orientation by means of pair production

A photon beam is now incident on the diamond crystal and is converted into electron pairs which are detected at equal energies, $y = 1/2$, and at a well defined photon energy k_0. A total intensity effect cannot be used in this case. However, the method of comparison of discontinuities in cross section with the pattern of Fig. 14 works also for PP. With δ defined by Eq. (2), the scaling factor A from Eq. (4) changes to:

$$A = y(1-y)\,\frac{4\,\pi\,k_0}{a\,M\,c^2} = \frac{\pi\,k_0}{a\,M\,c^2}, \quad \text{(PP)} \quad y = \tfrac{1}{2} \tag{45}$$

An advantage in studying PP lies in the fact that averaging effects are less critical than for BS because – as an inspection of Eqs. (1) and (2) shows – the minimum momentum transfer for PP, $y = 1/2$, is always larger than that for BS at the same energy. The ratio is already 4 at $x = 0.5$ and rises quickly for lower x. Thus for the same discontinuity the angle Θ is larger by the same ratio, as shown by Eq. (9). Moreover multiple scattering of the incident particles does not occur; therefore the reciprocal lattice points which contribute to the intensity are well defined by the primary direction. As a consequence the cross section for PP is less sensitive against errors in angle, so that the step heights for PP are a rather precise tool for the identification of the line. $\Delta J^c = J^{cu} - J^{cl}$, defined in Eq. (38), may be calculated in analogy to Eq. (27) from the equivalent formulas for PP. For $y = 1/2$ one obtains:

$$\Delta J^c = \frac{(2\,\pi)^4}{8\,a^5\,M\,c^2}\,|\,S\,|^2\,e^{-Ag^2}\,C(g^2)\;(n_2^2 + 2\,n_3^2). \tag{46}$$

Table 4 gives values for ΔJ^c for a number of lattice points in the vicinity of the origin. The parameters of orientation $\Phi_2{}^0$, $\Phi_3{}^0$ and m are thus determined by a comparison of the discontinuities in the pair cross section in height and position with the pattern of Fig. 14.

n_2	n_3	J^c (GeV^{-1})	n_2	n_3	J^c (GeV^{-1})
0	2	0.8884	4	4	0.1742
1	1	0.6356	5	1	0.1576
4	0	0.5182	3	3	0.1576
3	1	0.3548	8	0	0.1265
4	2	0.3540	8	2	0.1103
0	4	0.2658	0	6	0.1101
1	3	0.2214			

Table 4. PP, $y = 1/2$.

9. The Influence of Experimental Imperfections

It is beyond the scope of this paper to discuss quantitatively the various influences on the spectra due to experimental imperfections. We want to give a rough and qualitative idea only of possible deviations from the assumptions made in paragraph 1 and of their influence on the data presented for idealised conditions in the subsequent paragraphs. The primary energy scattering can be made so small that their influence can be neglected. Four effects will remain which tend to smear out the discontinuities and reduce the height of the peaks, particularly for small angles Θ. These are: primary divergence of the beam, multiple scattering in the crystal, mosaic structure of the crystal lattice, and mechanical vibrations of the target.

For BS the effects from multiple scattering and divergence are reduced by collimation up to the degree where the natural angular distribution $M c^2/E_0$ is dominant. There is experimental evidence from the measurements reported in ref. [9] that the mosaic spread is certainly smaller than 0.1 mrad if the diamond is cut from a well-grown octahedral crystal. Vibrations, although they are likely to occur, can be avoided by careful design of the support. It must be noted that the reduction in intensity does not only result from the uncertainty of orientation in $\Delta\Theta/\Theta$ but also and even stronger from the azimuthal error $\Delta\alpha \cong \Delta\Theta/\Theta$ connected with $\Delta\Theta$.

The PP is less sensitive to these imperfections because the angles involved are larger by a factor of at least four if equal energies k_0, E_0 are compared. In addition, multiple scattering of the incident particles does not occur, and the primary divergence can be reduced by collimation of the photon beam to a very low value. Therefore experimental results for coherent PP can be expected to agree with the data presented here to within a few percent, the slopes at the discontinuities being smaller than 0.1 mrad.

Acknowledgements

The basic computer program from which the data originate has been written by Dr. G. Bologna. We thank him for his various contributions to this work by discussions, suggestions, and calculations. We are also grateful to the operating staff of the DESY computer center, as well as to Miss Kuffner who compiled the calculations and made the drawings.

Anregung der Elektronenhülle des Rb^+ als Nachwirkung beim β-Zerfall von Kr^{85}

H. J. Andrä, K. Luchner und W. Schambeck

Physik-Department der Technischen Hochschule München, Teilinstitut Prof. H. Maier-Leibnitz

(Z. Naturforschg. **21 a**, 1987—1988 [1966]; eingegangen am 26. August 1966)

Beim β-Zerfall des Kr^{85} verbleibt der Elektronenhülle im Mittel etwa die Energie 80 eV [1], so daß bei ihrer Umordnung, wie in einer Anzahl theoretischer Arbeiten [2–6] gezeigt wird, Ionisation oder Anregung zu erwarten ist. Experimentell gesichert ist aber, daß bei 80% aller Zerfälle keine Ionisation auftritt [7]. Es entstehen also überwiegend Rb^+-Ionen, welche angeregt sein und dann unter Lichtemission in den Grundzustand übergehen können. Über den Nachweis einer solchen Lichtemission als Folge der Hüllenumordnung nach β-Zerfall sollen hier erste Ergebnisse mitgeteilt werden.

Aus einem Gefäß, das mit Kr^{85} angereichertem Krypton gefüllt war, wurden Photonen in Koinzidenz mit β-Teilchen des Kr^{85}-Zerfalls gemessen. Der Nachweis der einzelnen Photonen geschah durch einen rauscharmen, schnellen Photomultiplier (RCA 8575), dessen Ausgangsimpulse in einer hochempfindlichen Tunneldiodenschaltung geformt und mit den Ausgangsimpulsen eines schnellen β-Szintillationszählers einem Zeit-Amplituden-Konverter zugeführt wurden. Durch ein im optischen Strahlengang befindliches Interferenzfilter konnte bei jeder Einzelmessung ein enger Spektralbereich untersucht werden. Abb. 1 zeigt für einen solchen Spektralbereich die zeitliche Korrelation der β-Photonenkoinziden-

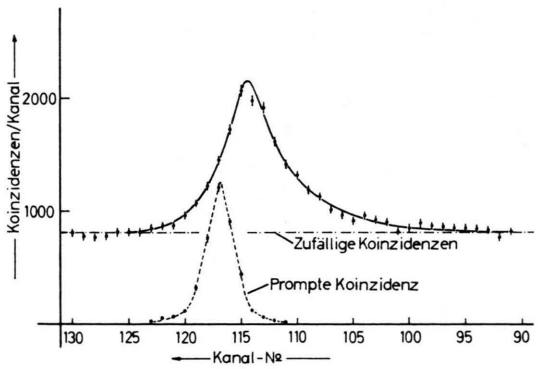

Abb. 1. β-Photon-Koinzidenz im Wellenlängenintervall 4110 Å bis 4180 Å. Zeitmaßstab: 1,9 nsec pro Kanalabstand.

[1] R. Serber u. H. S. Snyder, Phys. Rev. **87**, 152 [1952].
[2] A. Migdal, J. Phys. (USSR) **4**, 449 [1941].
[3] E. L. Feinberg, J. Phys. (USSR) **4**, 423 [1941].
[4] H. M. Schwartz, J. Chem. Phys. **21**, 45 [1953].
[5] P. Benoist-Gueutal, J. Phys. Rad. **16**, 595 [1955].
[6] J. S. Levinger, J. Phys. Rad. **16**, 556 [1955].
[7] A. H. Snell u. F. Pleasonton, Phys. Rev. **107**, 740 [1957].
[8] O. Laporte, G. R. Miller u. R. A. Sawyer, Phys. Rev. **38**, 843 [1931].